Materials Transactions, Vol. 47, No. 9 (2006) pp. 2254 to 2258
Special Issue on Porous and Foamed Metals —Fabrication, Characterization, Properties and Applications—

Laser Welding of Lotus-Type Porous Iron

Hiroyasu Yanagino[1,*], Takuya Tsumura[2], Hideo Nakajima[3], Soong-Keun Hyun[3] and Kazuhiro Nakata[2]

[1]*Division of Materials and Manufacturing Science, Graduate School of Engineering, Osaka University, Suita 565-0871, Japan*
[2]*Joining and Welding Research Institute, Osaka University, Ibaraki 567-0047, Japan*
[3]*The Institute of Scientific and Industrial Research, Osaka University, Ibaraki 567-0047, Japan*

A lotus-type porous iron (AISI 1018) that is fabricated by unidirectional solidification using the continuous zone melting technique in a nitrogen atmosphere under a pressure of 2.5 MPa, was welded by a Nd:YAG laser. The melting property of this was investigated to evaluate its melting characteristics at different laser powers and welding speeds. The weld bead surface of the lotus-type porous iron was rough with pits and dents irrespective of the pore growth direction. The remarkable effect of the pore growth direction on the penetration depth of the weld bead was not observed. This was due to the unstable weld bead formation caused by the relatively large-sized pores and the blowing of the remaining gas from the closed pores as well as the smaller anisotropy of the thermal diffusivity as compared to the copper and magnesium cases.
[doi:10.2320/matertrans.47.2254]

(Received February 28, 2006; Accepted July 7, 2006; Published September 15, 2006)

Keywords: *lotus-type porous iron, laser welding, penetration depth, effective thermal properties*

1. Introduction

Lotus root like (lotus-type) porous metals had been developed by Boiko *et al.*[1)] and Nakajima[2)] in the 1990s. The pores in this formed by a supersaturated gas that utilizes the difference in gas solubility between liquids and solids. These pores are aligned in one direction by unidirectional solidification and possess higher strength than conventional porous metals.[3,4)] The strength of these materials determined by tensile tests depends on the porosity and the pore growth direction, which is relative to the tensile direction.[5)] This is because of the significant stress concentration at the pore wall when the pore growth direction is perpendicular to the tensile direction. Lotus-type porous metals are expected to have industrial applications such as car materials, which require strength, lightweight, and functional properties. Therefore, a reliable joining technology such as welding is required to fabricate parts comprising identical lotus-type porous metals or dissimilar material such as nonporous metals. Researches on the welding of foamed aluminum have been reported for MIG arc welding and laser welding.[6–9)] We have already investigated the laser weldability of lotus-type porous copper[10)] and magnesium[11)] and have pointed out that weld formation was considerably influenced by the anisotropies of laser energy absorption and the thermal conductivities of lotus-type porous metals. In this study, we employed a Nd:yttrium-aluminium-garnet (Nd:YAG) laser welding in a lotus-type porous iron specimen. The effect of welding conditions and pore anisotropy on the penetration depth and the shape of the weld fusion zone was examined at different laser powers and welding speeds. This effect manifested itself in three different relationships—the laser-irradiation direction, the pore growth direction, and the welding direction.

*Graduate Student, Osaka University

Table 1 Nominal chemical compositions of AISI 1018.

C	Si	Mn	P	S
0.15–0.20%	<0.35%	0.60–0.90%	<0.030%	<0.050%

2. Experimental Procedure

Lotus-type porous iron plates made from AISI 1018 steel with a width of 40 mm, length of 500 mm, and thickness of 8 mm were prepared by the continuous zone melting technique in a pressurized nitrogen atmosphere at 2.5 MPa.[12–14)] Table 1 shows the nominal chemical compositions of AISI 1018. Figure 1 shows the appearance of the top view of the formed lotus-type porous iron (a), its cross section (b), and the test piece for laser welding (c) that was cut out from the porous plate since the pore growth direction was parallel to the specimen surface and machined to the flat surface. The average pore diameter and the porosity of the specimen were about 0.37 mm and 17%, respectively. Figure 2 shows schematic views of the weld specimen that exhibits co relationships among the pore growth direction, the laser beam irradiating direction, and the welding direction. Figure 2(a) shows the unidirectional pores both perpendicular to the top surface of the specimen and the welding direction; Fig. 2(b), the unidirectional pores both parallel to the top surface and the welding direction; and Fig. 2(c), the unidirectional pore parallel to the top surface and perpendicular to the welding direction.

The wavelength of the Nd:YAG laser beam is 1064 nm and is delivered by using an optical fiber of diameter 1.0 mm. This laser is irradiated the surface of the specimen at an angle of 58° to prevent damage to the optics by the reflected laser beam. Argon with a flow rate of 4.2×10^{-4} m^3 s^{-1} was used as the shielding gas. The diameter of the laser beam on the specimen surface was about 1.0 mm. In this study, the process parameters selected were the laser beam power and the welding speed; they were varied in the range of 1.0 to 2.0 kW

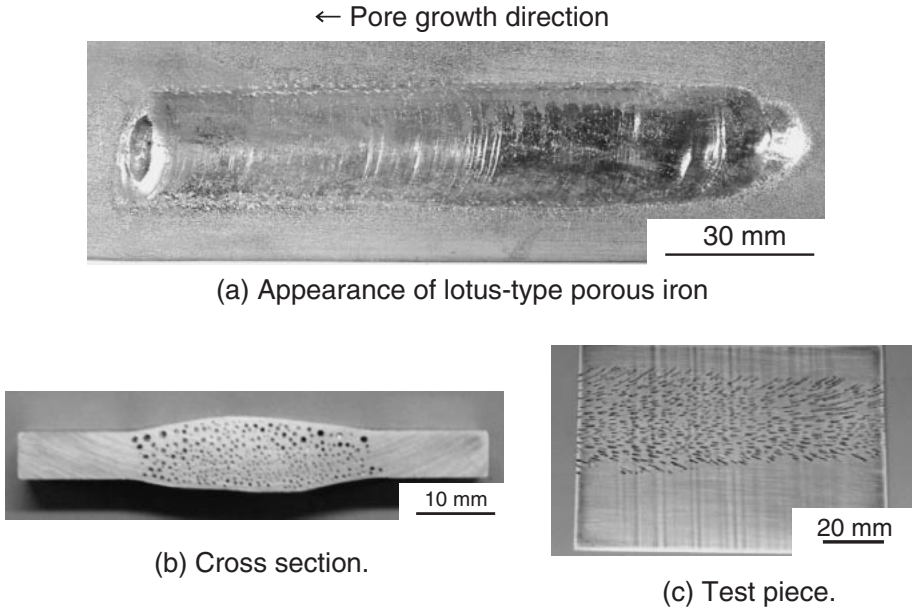

Fig. 1 Appearance of the top view of the formed lotus-type porous iron prepared by the continuous zone melting technique (a), its cross section (b), and the test piece for laser welding (c).

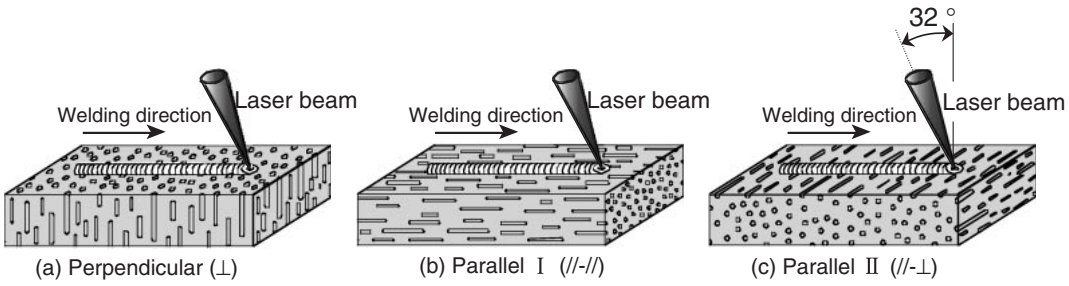

Fig. 2 Schematic views of the lotus-type porous iron specimens showing different combinations of welding directions and pore growth directions.

and 1 to 3 m/min, respectively. The effective power irradiated on the specimen surface was approximately 87% that of the laser beam because the optical system of the laser unit absorbs the energy of the laser. The cross sections of the laser welds were observed with an optical microscope and the Vickers microhardness was measured at a load of 1.96 N. In order to investigate the remaining gas in the closed pores of the porous plate, a 2 mm diameter hole was drilled in the test piece in the vacuum chamber under 6×10^{-6} Pa and the residual gas in the pore was analyzed using a mass spectrometer (ANELVA Corporation, AGS-7000 improved version).[10)]

3. Result and Discussion

Figure 3 shows the formation of 2 mm thick laser-welded specimens at a constant laser beam power of 1.0 kW and a welding speed of 1 m/min. Here, original unidirectional pores are observed in parts other than the weld bead of the porous iron; they are indicated like holes or grooves and are indicated by the black arrows in Fig. 3. As shown in Fig. 3, a smooth weld bead was obtained on nonporous iron, while the weld bead of the porous iron exhibited a rough surface with dents or pits. This is probably caused due to the volume reduction caused by the melting of the porous iron. The black welded bead surface observed in the two parallel cases suggests the blowing of the remaining gas into the closed pores of the molten metal; this also caused the Ar gas shield to break and resulted in its reaction with air. Table 2 shows the result of the analysis of the gas remaining in the base metals by drilling at their surface. Nitrogen was primarily detected in the remaining gas in addition to hydrogen from the closed pores. Therefore, pretreatment is required for eliminating this gas in order to ensure successful fusion welding for this type of porous metal.

Figure 4 shows the cross-sectional view of the weld specimens shown in Fig. 3 and the original unidirectional pores indicated by the black arrows. The penetration depth in the lotus-type porous iron was slightly greater than that in the nonporous iron. It is considered that the relative density, namely, the heat capacity and volume reduction of the porous iron is lower than that of the nonporous iron. In order to evaluate the influence of the pore growth direction more accurately, the penetration depths of the weld bead for three types of pore directions were measured; they are summarized in Fig. 5 for four different welding conditions. Here, the

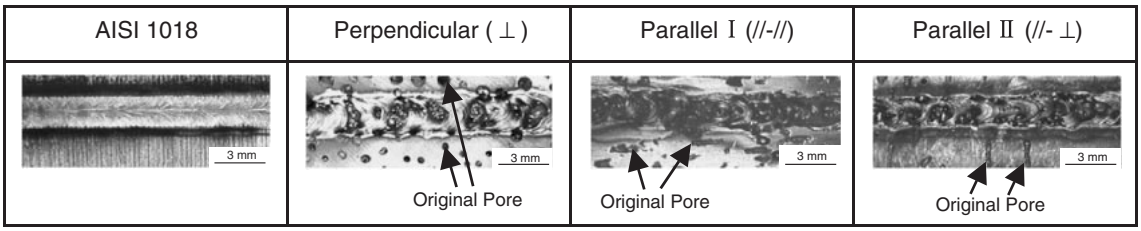

Fig. 3 Appearance of laser weld beads on the nonporous iron (AISI 1018) and lotus-type porous iron; pore directions perpendicular (⊥), parallel I (//-//), and parallel II (//-⊥) to the specimen surface at a laser power of 1.0 kW and welding speed of 1 m/min.

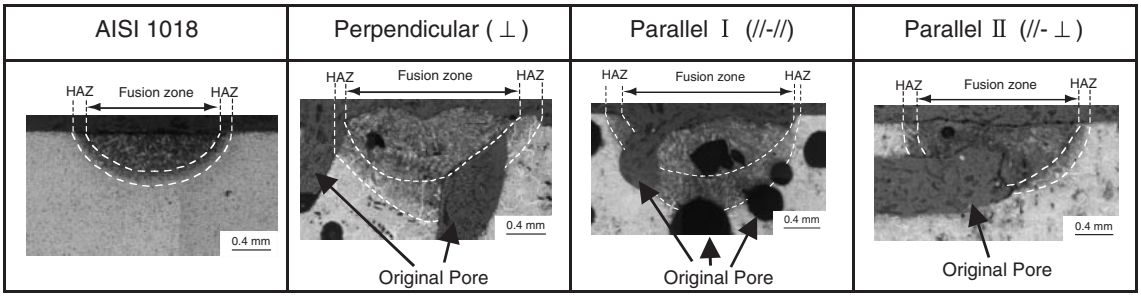

Fig. 4 Cross section of the laser weld beads of the nonporous iron (AISI 1018) and lotus-type porous iron; pore directions perpendicular (⊥), parallel I (//-//), and parallel II (//-⊥) to the specimen surface at a laser power of 1.0 kW and welding speed of 1 m/min.

Table 2 Summary of the gas analysis results in the pores of a test piece when the pore direction is parallel to the specimen surface.

Remaining gas	No. 1	No. 2
H_2	3.8	—
CH_3	—	—
H_2O	—	0.3
N_2	95.0	99.7
O_2	—	—
Ar	—	—
CO_2	1.2	<0.1
Approximate gas volume (ml)	8×10^{-6}	2×10^{-4}

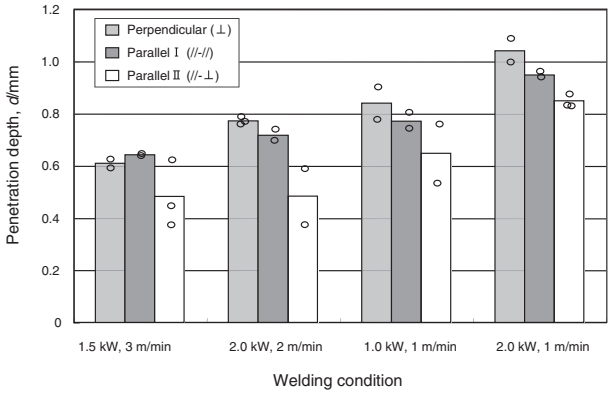

Fig. 5 Comparison of the penetration depth of the laser weld bead for the lotus-type porous iron under different welding conditions; pore directions perpendicular (⊥), parallel I (//-//), and parallel II (//-⊥) to the specimen surface.

penetration depth is defined as the measured depth of fusion zone at the three different cross sections of each specimen, and the bar graph shows the average value. The penetration depth in the perpendicular (⊥) case was slightly higher than that in the parallel I (//-//) case and the parallel II (//-⊥) case; however, the remarkable difference observed in the case of the lotus-type porous copper[10] and magnesium[11] was not observed in these results. In general, many large pores greater than 0.5 mm in diameter prevented the formation of the smooth penetration of weld as well as the blowing of the remaining gas. It can be pointed out that in order to obtain a smooth weld bead, a finer pore size and the elimination of the remaining gas in the closed pores are required before welding.

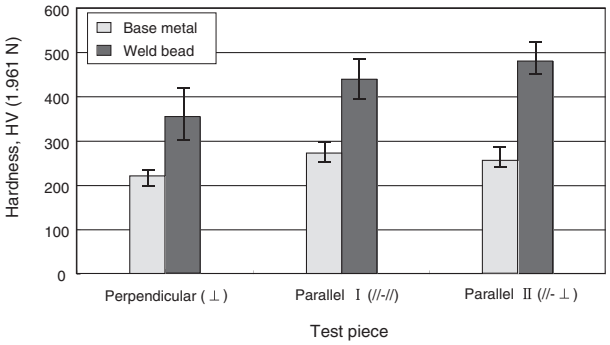

Fig. 6 Hardness of the base metal and weld bead for different pore directions at a laser power of 2.0 kW and welding speed of 2 m/min.

The mean values of the Vickers hardness of the perpendicular (⊥), parallel I (//-//), and parallel II (//-⊥) cross sections at a laser power of 2.0 kW and welding speed of 2 m/min are shown in Fig. 6. Irrespective of their pore directions, the hardness of the weld bead increased as compared with that of the base metal. This is due to the martensitic structure formed in the weld bead due to the rapid cooling rate of the laser welding, as shown in Fig. 7(a). The comparison with ferrite in the base metal is shown in Fig. 7(b).

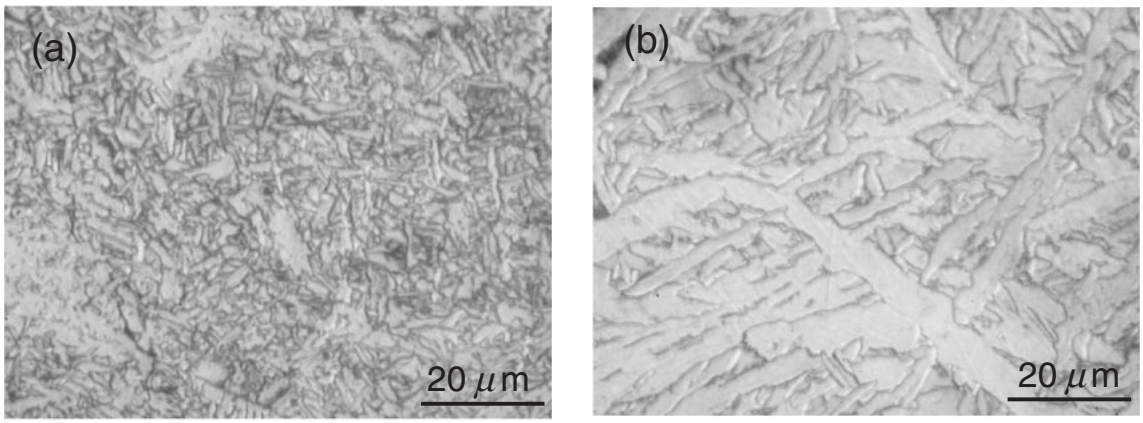

Fig. 7 Microstructure of the cross sections of the weld metal (a) and base metal (b) at a laser power of 2.0 kW and welding speed of 2 m/min.

Table 3 Reflectivity and thermal properties of iron (S35C), copper, and magnesium at room temperature.[15,16]

	Reflectivity (%)	ρ_n (kg/m^3)	$C_{p\,n}$ (J/kg·K)	λ_n (W/m·K)	ε (%)	$\alpha_{eq}^{//}$ (m^2/s)	$\alpha_{eq}^{\perp}$ (m^2/s)
Fe (S35C)	57	7859	464	43.1	17	1.18×10^{-5}	1.01×10^{-5}
Cu	95	8951	382	400	30	11.7×10^{-5}	8.98×10^{-5}
Mg	74	1737	1063	156	35	8.44×10^{-5}	6.25×10^{-5}

In the previous reports,[10,11] it has been pointed out that the weld formation was significantly influenced by the anisotropies of laser energy absorption and the thermal conductivities of lotus-type porous metals. Thus, the penetration depth of the pore growth direction perpendicular to the laser irradiated surface was appreciably greater than that observed the other cases. However, a remarkable difference was not observed in these results for the lotus-type porous iron. Here, we discuss the reason for this. Table 3 summarizes the reflectivity and the thermophysical properties of iron (S35C), copper, and magnesium at room temperature.[15,16] According to the report on lotus-type porous copper,[10] the parallel II (//-⊥) specimen exhibited almost no weld bead with little molten copper due to a high reflectivity of approximately 95%.[15] On the other hand, the perpendicular (⊥) specimen showed that the weld bead fully penetrated till the bottom of the specimen. It was considered that the heat input to the porous copper increased due to the multiple reflection of the laser beam along the pore wall side when the beam irradiated the open pores. However, the remarkable difference in the penetration depth was not reported for the lotus-type porous magnesium[11] in which reflectivity is about 74%.[15] In the case of the lotus-type porous iron, the reflectivity is about 57%[15] and is much lower than that of copper. Therefore, this suggests that the effect of the multiple reflection of the laser beam on the anisotropy of the penetration depth of the lotus-type porous iron like magnesium is much lower than that of copper. The inherent anisotropy in the thermal properties of a lotus-type porous metal probably produces the anisotropy in the penetration depth of the weld bead with regard to the pore growth direction. In order to describe the thermal characteristics of a material, the thermal diffusivity α is used. This is defined as follows:[17]

$$\alpha = \lambda/(\rho \cdot C_p), \tag{1}$$

where λ is the thermal conductivity; ρ, the density; and C_p, the specific heat. Moreover, the equivalent density, equivalent specific heat, and thermal conductivity of the lotus-type porous metal are described by the following equations.[11]

$$\rho_{eq} = (1-\varepsilon)\rho_n, \quad C_{p\,eq} = C_{p\,n}, \tag{2}$$

$$\lambda_{eq}^{//} = (1-\varepsilon)\lambda_n, \quad \lambda_{eq}^{\perp} = (1-\varepsilon)\cdot(1+\varepsilon)^{-1}\cdot\lambda_n. \tag{3}$$

Here, ρ_{sub}, $C_{p\,sub}$, and λ_{sub}^{dir} are the density, specific heat, and thermal conductivity, respectively. The subscript *sub* of *eq* and *n* implies the equivalent property and the nonporous property, respectively, and the superscript *dir* of // and ⊥ indicates the direction parallel and perpendicular to the unidirectional pores, respectively. ε is the pore volume content rate. Therefore, the equivalent thermal diffusivity parallel to the unidirectional pores $\alpha_{eq}^{//}$ and the equivalent thermal diffusivity perpendicular to the unidirectional pores $\alpha_{eq}^{\perp}$ for the lotus-type porous iron, copper, and magnesium at room temperature can be estimated by using eqs. (1), (2), and (3). These estimated values as well as the thermal properties for the nonporous metals are listed in Table 3. The equivalent thermal diffusivities in the case of iron are $\alpha_{eq}^{//}$ of 1.18×10^{-5} (m^2/s) and $\alpha_{eq}^{\perp}$ of 1.01×10^{-5} (m^2/s). A comparison of the copper and magnesium case shows that the difference between these equivalent values is very small. Therefore, it can be evaluated that the effect of the anisotropic properties much smaller than that in the copper and the magnesium cases.

In the laser welding of the lotus-type porous iron, prevention of volume reduction due to melting the pores by providing the filler metal, pretreatment for eliminating the remaining gas in the closed pores by heat treatment, and

smaller diameter of the pores are required for ensuring successful fusion welding.

4. Conclusive Remarks

The melting property of lotus-type porous iron (AISI 1018) has been investigated by Nd:YAG laser welding with a laser power of 1–2 kW and a welding speed of 1–3 m/min with argon as the shielding gas to evaluate the effect of the pore growth direction on the penetration depth of the weld bead. The results obtained are summarized as follows:

(1) The weld bead surface of the lotus-type porous iron was rough with pits and dents irrespective of the pore growth direction—perpendicular (⊥), parallel I (//-//), or parallel II (//-⊥) to the specimen surface. This is due to volume reduction on melting the porous metal and blowing the remaining gas from the closed pores.

(2) The penetration depth in the perpendicular (⊥) case was slightly greater than that in the parallel I (//-//) and parallel II (//-⊥) cases. However, the remarkable effect of the pore growth direction on the penetration depth of the weld bead, as already observed in the case of the lotus-type porous copper and magnesium, was not observed in this study. This was due to the unstable weld bead formation caused by the relatively large-sized pores and the blowing of the remaining gas from the closed pores as well as the smaller anisotropy of the thermal diffusivity as compared to the copper and magnesium cases.

Acknowledgment

This research was supported as part of the entrusted project "development of lightweight high stiffness structural materials and evaluation technology" for the "advanced machining system development project" in the fiscal year 2005 consigned by NEDO.

REFERENCES

1) L. V. Boiko, V. I. Shapovalov and E. V. Chernykh: Sov. Powder Metal. Met. Ceram. **30** (1991) 78–81.
2) H. Nakajima: Prod. Tech. **51** (1999) 60–62.
3) T. Ogushi, H. Chiba, H. Nakajima and T. Ikeda: J. Appl. Phys. **95** (2004) 5843–5847.
4) S. K. Hyun and H. Nakajima: Mater. Trans. **43** (2002) 526–531.
5) S. K. Hyun, K. Murakami and H. Nakajima: Mater. Sci. Eng. A **299** (2001) 241–248.
6) A. G. Pogibenko, V. Y. Konkevich, L. A. Arbuzova and V. I. Ryazantsev: Weld. Int. **15** (2001) 312–316.
7) T. Bernard, J. Burzer and H. W. Bergmann: J. Mater. Process. Technol. **115** (2001) 20–24.
8) Th. Bollinghaus and W. Bleck: *Cellular Metals and Metal Foaming Technology*, (Verlag MIT Publishers, Bremen, 2001), pp. 495–500.
9) H. Haferkamp, J. Bunte, D. Herzog and A. Ostendorf: Sci. Technol. Weld. Joining **9** (2004) 65–71.
10) T. Murakami, K. Nakata, T. Ikeda, H. Nakajima and M. Ushio: Mater. Sci. Eng. A **357** (2003) 134–140.
11) T. Tsumura, T. Murakami, S. K. Hyun, H. Nakajima and K. Nakata: Mat. Sci. Forum **502** (2005) 499–504.
12) S. K. Hyun and H. Nakajima: Advanced Eng. Mater. **4** (2002) 741–744.
13) M. Tane, T. Ichitsubo, H. Nakajima, S. K. Hyun and M. Hirao: Acta Mater. **52** (2004) 5195–5201.
14) S. K. Hyun, T. Ikeda and H. Nakajima: Sci. Technol. Adv. Mater. **5** (2004) 201–205.
15) E. A. Brandes: *Smithells Metal Reference Book, 6th ed.*, (1983), p. 17–7.
16) K. Kobayasi: J. Japan Soc. Mechanical Engineers **81** (1978) 452–457.
17) A. L. Philips Ed.: *Welding Handbook, Sixth ed., Section One, Fundamentals of Welding* (1968), p. 2.4.